*ECS Electrochemistry Letters*, **2** (5) A43-A45 (2013)
2162-8726/2013/2(5)/A43/3/$31.00 © The Electrochemical Society



# Probing Electrode Losses in All-Vanadium Redox Flow Batteries with Impedance Spectroscopy

**Che-Nan Sun,[a,z] F. M. Delnick,[b,*] D. S. Aaron,[c] A. B. Papandrew,[c] M. M. Mench,[a,c,*] and T. A. Zawodzinski[a,c,**]**

[a]*Physical Chemistry of Materials Group, Emissions and Catalysis Research Group, Oak Ridge National Laboratory, Oak Ridge, Tennessee 37831, USA*
[b]*Power Sources Technology Group, Sandia National Laboratory, Albuquerque, New Mexico 87185, USA*
[c]*Department of Chemical and Biomolecular Engineering, Department of Mechanical, Aerospace, and Biomedical Engineering, University of Tennessee, Knoxville, Tennessee 37996, USA*

We report on single-electrode electrochemical impedance spectroscopy studies of an all-vanadium redox battery using a dynamic hydrogen reference electrode. The negative electrode, comprising the $V^{2+}/V^{3+}$ couple, contributes approximately 80% of the total cell overpotential during discharge. The impedance spectra measured at the negative electrode exhibit high-frequency, semicircular arcs which correspond to the double layer capacitance in parallel with a faradaic resistance. The faradaic resistance decreases in magnitude with increasing polarization. Integration of the current-dependent faradaic resistance quantifies the fraction of the overvoltage that is attributed to the kinetic limitations of the charge transfer reaction.
 [DOI: 10.1149/2.001305eel] 

Manuscript submitted November 29, 2012; revised manuscript received January 14, 2013. Published February 15, 2013. This was Paper 399 presented at the Honolulu, Hawaii, Meeting of the Society, October 7–12, 2012.

Redox flow batteries (RFB) are considered potential candidates for grid-integrated storage of energy generated by wind, solar and other sustainable resources.[1–4] However, adoption of RFBs for this application is contingent upon reducing overall system cost. In the well-known case of the aqueous all-vanadium RFB(VRFB),[5–10] both the energy storage medium and the energy conversion cells contribute significantly to the system cost.[11] One key route to cost reduction is an increase of cell current density at the desired operating voltage, permitting decreased cell and/or stack size. In previous work,[12] we demonstrated a "zero-gap" cell configuration to achieve a greatly improved power density, in part due to large reductions in the ohmic resistance of the cell. However, ohmic losses are not sufficient to account for the total cell overpotential, which remains substantial.

Though ohmic losses in the "zero-gap" cell configuration are largely governed by the ion-exchange membrane separator, the remaining overpotentials, broadly comprising charge transfer kinetics and mass transport, originate in electrode processes. These processes can be separated at the cell level with single-electrode methods through the use of a reference electrode. Using this approach, surprising asymmetries in the behavior of VRFB systems have already been revealed.[13]

In this work, we demonstrate the use of electrochemical impedance spectroscopy with a dynamic hydrogen reference electrode to obtain more detailed information on the relative magnitude of loss mechanisms in VRFB electrodes.

## Experimental

Vanadium electrolyte solutions containing 1M vanadium ions and 5M sulfuric acid were prepared from vanadium (IV) sulfate oxide hydrate (99.9%, Alfa Aesar) and sulfuric acid, (93-98% Alfa Aesar) diluted appropriately with deionized water. The solutions were charged at 1.8 V using a protocol described previously.[12]

Battery testing was conducted using a 5 $cm^2$ single cell (Fuel Cell Technologies). The cell hardware consisted of aluminum end plates, gold-plated current collectors, and graphite blocks with a single serpentine flow field for electrolyte distribution. Carbon paper (SGL 10AA, 400 microns thick, $<12\ m\Omega\ cm^2$) was used for both the positive and negative electrodes. Two pieces of Nafion 117 (Ion Power) were used as the separator. A dynamic hydrogen reference electrode[13] was inserted between the two Nafion membranes.[14]

PTFE-coated fiberglass sheet (Fuel Cell Technologies) served as the incompressible cell gasket. The thickness of the gasket was chosen to achieve 20% compression of the electrode material upon cell closure.

Electrochemical measurements were performed using a Bio-Logic HCP-803 high current potentiostat. Electrochemical impedance spectroscopy (EIS) was used to characterize the individual responses of the positive and the negative electrode to polarization. The electrode of interest was polarized for two minutes to reach a steady state current. The impedance of the electrode was then measured using a 5 mV sinusoidal perturbation superimposed onto the DC polarization potential. After the impedance measurement, the DC polarization was increased incrementally to establish the steady state polarization curve for the individual electrode with a complex impedance spectrum measured at each point on the curve. The reference electrode response was checked by comparing the summation of the positive and the negative spectra with that of the full cell response, indicating the reference electrode does not interfere with the impedance spectrum at the frequency up to 60 kHz. Measurements were performed at 17°C (room temperature as monitored by a K-type thermocouple).

The electrolyte in each compartment of the individual electrodes was not recirculated. Instead, the outlet from each electrode was directed to a separate outlet bottle to maintain a constant state of charge. As a result, the open circuit voltage before each discharge was equal to the open circuit voltage after the discharge. A constant flow rate of 1.5 mL/min was maintained with a gravity siphon by placing each inlet bottle 25 cm above its corresponding outlet bottle. This stoichiometric flow rate is seven times the highest current used in this study. This procedure allowed us to maintain a constant state of charge ~55% throughout the polarization measurements and to minimize noise associated with solution pumping. To eliminate air oxidation of the negative electrode reactants, the solutions in each bottle were covered by a 'blanket' of flowing ultra-high purity nitrogen.

## Results and Discussion

Individual electrode polarizations with respect to the reference were obtained as a function of cell current, and a full cell discharge polarization curve was constructed from the sum of these voltages (Figure 1). The loss from each electrode is asymmetric, and the processes at the negative side ($V^{2+}/V^{3+}$) account for the majority of the loss, in agreement with other recently published results.[13] We note the early onset of limiting current behavior in the polarization curve, presumably a consequence of the low flow rate and minimal convection obtained from the gravity-fed electrolyte. We comment in passing that

*Electrochemical Society Active Member.
**Electrochemical Society Fellow.
zE-mail: sunc@ornl.gov

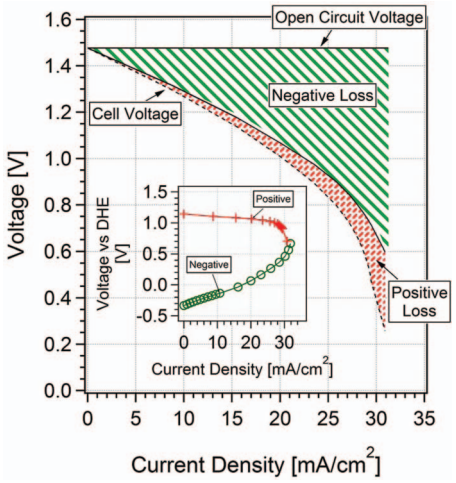


**Figure 1.** Cell polarization curve with the losses isolated from each electrode using DHE, including IR, kinetic and mass transport losses. Dash line: cell voltage, red: voltage loss from the positive electrode, green: voltage loss from the negative electrode. Condition: flow rate ~1.5 mL/min, state of charge ~55%, and temperature at 17°C.

the results presented here represent low mass transfer rates. It is beyond the scope of this note, which focuses on the method, to describe the full flow rate dependence of the impedance behavior.

To investigate the electrode voltage losses further, electrochemical impedance spectroscopy was conducted on each half-cell in an attempt to isolate the processes contributing to the total cell overpotential. Nyquist impedance plots at various overpotentials for the positive and the negative electrode are shown in Figure 2 and Figure 3, respectively. Since the reference electrode was sandwiched between two Nafion 117 membranes, the ohmic resistance, $R_{hf}$ (measured at the high frequency intercept with the real (x) axis) is attributed to the resistance of one membrane for each half-cell.

At the negative electrode, the semicircular arc (Figure 2) can be represented by a faradaic charge transfer resistance, $R_{ct}$, in parallel with a double-layer capacitance, $Q_2$. The double layer capacitance did not change appreciably with polarization, however, the charge transfer resistance decreased exponentially with increased polarization, consistent with Tafel kinetics. $R_{hf,}$ $R_{ct}$, and $Q_2$ can be quantified by fitting the data in Figure 2 to the equivalent circuit shown as the

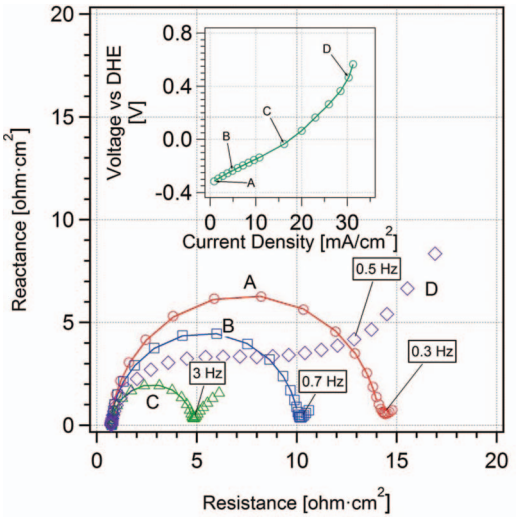


**Figure 2.** Selected Nyquist plots of the overpotentials at 20 mV(A), 100 mV(B), 300 mV(C), 800 mV(D) on the negative electrode. Line: fitting result. Sub-graph: Polarization curve of the negative electrode.

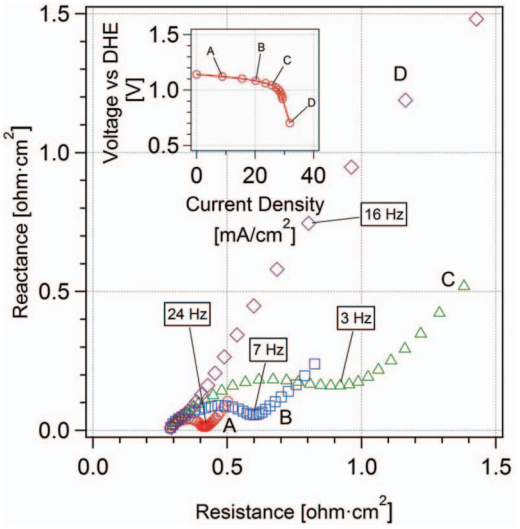


**Figure 3.** Selected Nyquist plots of the overpotentials at 20 mV (A), 60 mV (B), 100 mV (C), 440 mV (D) on the positive electrode. Top sub-graph: Polarization curve of the positive electrode.

sub-graph in Figure 4. At currents higher than point "C" on the polarization curve in Figure 4 (16 mA/cm$^2$), the charge transfer resistance became convoluted with an undefined low frequency mass transport impedance and we could no longer resolve $R_{ct}$ from the impedance spectrum. Therefore, at polarizations above point "C", we estimated $R_{ct}$ from the extrapolation of the exponential fit of the $R_{ct}$ data below point "C" in Figure 4.

Charge transfer resistance is defined by Equation 1[15]

$$\frac{d\eta_{ct}}{di} = R_{ct} \qquad [1]$$

where $\eta_{ct}$ is the overpotential attributed to the charge transfer process and $i$ is the current density. Thus $\eta_{ct}$ can be obtained by integrating $R_{ct}$ with respect to current density. The charge transfer component of the overvoltage can, therefore, be resolved from the total overvoltage at the negative electrode.

On the positive electrode (Figure 3), the ohmic loss of the positive half-cell can be differentiated using the high frequency intercept.

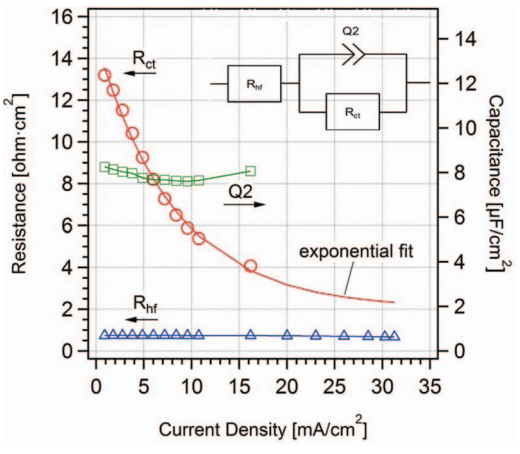


**Figure 4.** The charge transfer, the ohmic resistance and the capacitance plotted as a function of current density for the negative electrode. Sub-graph: the equivalent circuit for the fitting. $R_{ct}$: charge transfer resistance (circles). $R_{hf}$: high frequency resistance (triangles). Q2:double-layer capacitance fitted as a constant phase element(squares). In particular, $R_{ct}$ and $R_{hf}$ were normalized by the cell geometric area which is 5 cm$^2$. Q2 was normalized by the surface area obtained through a 7-point BET measurement. For the carbon paper in this work, the measured BET surface area is (0.65 ± 0.05) m$^2$/g.

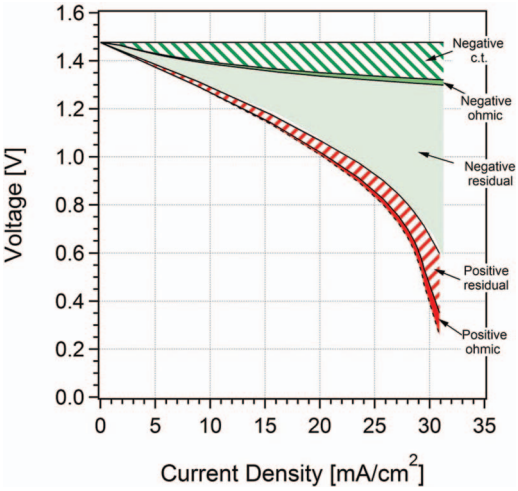


**Figure 5.** Resolved component contributing to the voltage loss in the system studied. Dash line: cell voltage. c.t.: charge transfer. Negative residual: negative loss with the charge transfer and the ohmic losses for the negative half-cell subtracted. Positive residual: positive loss with the ohmic loss for the positive half-cell subtracted.

However, for resolving the kinetic overvoltage, the complication rises due to the strongly distorted high-frequency arcs. In this case, it is difficult, if not impossible, to accurately estimate the resistance and the capacitance associated with the process. Work is currently ongoing to investigate the positive electrode in more detail.

As the charge transfer resistance for the negative electrode and the ohmic overpotential for each half-cell can be differentiated from the total loss, we therefore can plot the resolved components as a function of current density as shown in Figure 5. Since the $R_{ct}$ of the negative electrode decreases exponentially as current increases, the loss accounts for a significant portion of the overall loss at the low current region and stays nearly invariant at high current region. This implies that the charge transfer process is crucial as the battery operates under high efficiency condition. The observed relative magnitudes of the kinetic losses agrees well with recent polarization measurements.[13] The ohmic loss merely contributes a small segment of the total loss throughout the current range in this work. This is because the current of operation is relatively small in the system studied. Since the ohmic overvoltage is proportional to the operating current, we would expect the ohmic loss to become more significant when operating at high power/current region. In a previous study, high performance was achieved by feeding solution using a peristaltic pump at higher flow rate.[12] More convection can be created in this case and thus aid the diffusion process. However, a slower flow rate was performed in this work. We would expect the mass transport loss to be more pronounced in this system causing a poorer performance. The most salient feature of the results shown in Figure 5 is the substantially larger loss associated with the negative electrode in this system. Both kinetic and residual mass transfer losses are substantially higher. Further work is in progress to understand this observation.

## Conclusions

We demonstrate the use of electrochemical impedance spectroscopy with a dynamic hydrogen reference electrode to obtain more detailed information on the relative magnitude of loss components in VRFB electrodes. Over a portion of the polarization curve, the spectra derived from the negative electrode exhibit high-frequency semicircular arcs that decrease in impedance with increasing polarization, suggesting a loss ascribed to a kinetic process. The overpotential owing to this kinetic process is resolved yielding a quantified proportion of the total voltage loss.

## Acknowledgments

The authors gratefully acknowledge the support of the US Department of Energy Office of Electricity Storage Systems Program and the University of Tennessee Governor's Chair Fund for support of this work.

## References

1. C. Ponce de León, a. Frías-Ferrer, J. González-García, D. a. Szánto, and F. C. Walsh, *Journal of Power Sources*, **160**, 716 (2006).
2. Z. Yang, J. Zhang, M. C. W. Kintner-Meyer, X. Lu, D. Choi, J. P. Lemmon, and J. Liu, *Chemical Reviews*, **111**, 3577 (2011).
3. W. Wang, S. Kim, B. Chen, Z. Nie, J. Zhang, G.-G. Xia, L. Li, and Z. Yang, *Energy & Environmental Science*, **4**, 4068 (2011).
4. A. Z. Weber, M. M. Mench, J. P. Meyers, P. N. Ross, J. T. Gostick, and Q. Liu, *Journal of Applied Electrochemistry*, **41**, 1137 (2011).
5. M. Kazacos, M. Cheng, and M. Skyllas-Kazacos, *Journal of Applied Electrochemistry*, **20**, 463 (1990).
6. M. Rychcik and M. Skyllas-Kazacos, *Journal of Power Sources*, **22**, 59 (1988).
7. M. Rychcik and M. Skyllas-Kazacos, *Journal of Power Sources*, **19**, 45 (1987).
8. M. Skyllas-Kazacos, *Journal of The Electrochemical Society*, **133**, 1057 (1986).
9. E. Sum and M. Skyllas-Kazacos, *Journal of Power Sources*, **15**, 179 (1985).
10. C. Fabjan, J. Garche, B. Harrer, L. Jörissen, C. Kolbeck, F. Philippi, G. Tomazic, and F. Wagner, *Electrochimica Acta*, **47**, 825 (2001).
11. M. Moore, J. Watson, T. A. Zawodzinski Jr., M. Zhang, and R. M. Counce, Capital Cost Sensitivity Analysis of an All-Vanadium Redox-Flow Battery, in *ECS Transactions*, p. 1 (2012).
12. D. S. Aaron, Q. Liu, Z. Tang, G. M. Grim, a. B. Papandrew, a. Turhan, T. a. Zawodzinski, and M. M. Mench, *Journal of Power Sources*, **206**, 450 (2012).
13. D. S. Aaron, Z. Tang, J. S. Lawton, A. P. Papandrew, and T. A. Zawodzinski Jr., In Situ Single Electrode Studies of an All-Vanadium Redox Flow Battery, in *ECS Transactions*, p. 43 (2012).
14. D. S. Aaron, C. Sun, M. Bright, A. B. Papandrew, M. M. Mench, and T. A. Zawodzinski, (2012). submitted to EEL.
15. A. Parthasarathy, *Journal of The Electrochemical Society*, **139**, 1634 (1992).